International Journal of Advancements in Mechanical and Aeronautical Engineering – IJAMAE
Volume 1 : Issue 1
Publication Date : 09 January 2014

Position Control for an SMA Actuator Based on Inverse Model for Compensation

[Junfeng Li, Hiroyuki Harada]

***Abstract*—In this paper, a feedforward-feedback controller is used to control the position of an SMA actuator based on a modified Liang and Rogers inverse model, considering both the major and minor hysteresis loops. First a modified Liang and Rogers model of an SMA wire actuated by an electric current is derived and experiments are used to validate the model and to identify the parameters governing its behavior. Then the feedforward part of the proposed control system, which is based on this inverse model, is used to compensate the hysteresis effect, and a PID controller is added to the feedforward controller to increase the accuracy as well as reduce the steady state errors in the position control process. Experimental results demonstrate that the proposed control system performs better than when only a traditional PID controller is used.**

***Keywords*—SMA actuator, inverse hysteresis compensation, position control**

I. Introduction

Shape memory alloys (SMA) are metallic alloys which deform at low temperatures and return to the original undeformed state when heated to higher temperatures. The shape memory effect is a consequence of a reversion in the crystalline structure between the low temperature and high temperature phases, which are respectively called the martensite and the austenite of the SMA. The martensite phase is nonsymmetric and relatively soft, while the austenite phase is symmetric and relatively hard. Already, SMA have been used in a variety of actuation applications because of advantages such as excellent power-to-mass ratios, reliability, and silent actuation. These applications include mobile robots [1], microrobot manipulation [2], smart structures [3], and artificial muscles [4, 5, 6]. However, the ability of SMA actuators to memorize a specific shape is the result of physical changes which occur in a highly nonlinear fashion, introducing significant hysteresis in the actuator response and making it difficult to model and control the SMA actuators.

In this paper, first a successful empirical relation proposed by Liang and Rogers [7] is introduced in order to model the major hysteresis behavior of SMA actuators, which considers the amount of the austenite fraction transformed at a temperature. Based on this empirical relation, a modified Liang and Rogers model is demonstrated to show the major and minor hysteresis behaviors.

Junfeng Li, Hiroyuki Harada, Faculy of Engineering
Hokkaido University
Japan
lijunfeng@ec.hokudai.ac.jp

An experimental set-up used for verification of the modeling and tracking control system is presented and a series of tests are conducted to identify the parameters of the modified Liang and Rogers model. Subsequently, the formulation of the modified Liang and Rogers inverse model is presented for compensation of the hysteresis effect in SMA actuators based on the analytically invertible property of this model. Successively, the modified Liang and Rogers inverse model is applied to the SMA control system to reduce its hysteresis in real-time tracking control, in addition to the use as a feedback controller [8]. In the experimental tests, the results with the hysteresis compensation perform better and the tracking control performance is greatly improved in comparison with the case in which only a traditional PID controller is applied.

II. Modeling the Major and Minor Hysteresis Loops

First, The SMA may be seen as a smart material that changes shape due to changes in temperature. Instead of controlling the temperature by a Peltier device, this paper uses electricity to heat the SMA wire. The wire gains heat energy from the electrical current, and loses part of it to the environment. As suggested in Fig. 1, this and other models consider an SMA element as a three-element system in which thermal energy is concerted into a phase transformation and then into mechanical work. In this section, a mathematical model of the SMA actuator is introduced, including the major and minor hysteresis loops.

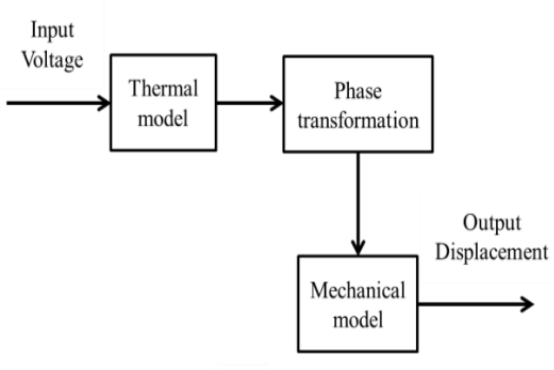

Figure. 1 Block diagram of the SMA

A. Thermal model

For a spring-biased SMA wire, the thermal model for the input voltage V and the output temperature T is a first-order system given by

$$\rho \cdot c \frac{\pi d_0^2 L_0}{4} \cdot \frac{dT}{dt} = \frac{V^2(t)}{R} - \pi d_0 L_0 h(T - T_{amb}) \quad (1)$$

where ρ is the density of the SMA; c is the specific heat coefficient; L_0 is the length of the SMA wire; d_0 is cross-sectional diameter of the SMA; V is the voltage applied; R is the resistance; h is the convection heat transfer coefficient, and T_{amb} is the ambient temperature.

B. Phase transformation model

During the heating process, a phase transformation occurs from martensite to austenite, while during the cooling process, the opposite transformation occurs, and SMA wires show a hysteresis effect during both phase transformations. Basic equations proposed by Liang and Rogers to model these transformations as functions of temperature are given below

$$\varepsilon_{ah} = \begin{cases} 1 & T > T_{AF} \\ 0.5\left[1 - \cos \pi \left(\frac{T - T_{AS}}{T_{AF} - T_{AS}}\right)\right] & T_{AS} \le T \le T_{AF} \\ 0 & T < T_{AS} \end{cases} \quad (2)$$

$$\varepsilon_{ac} = \begin{cases} 1 & T > T_{MS} \\ 0.5\left[1 - \cos \pi \left(\frac{T - T_{MF}}{T_{MS} - T_{MF}}\right)\right] & T_{MF} \le T \le T_{MS} \\ 0 & T < T_{MF} \end{cases} \quad (3)$$

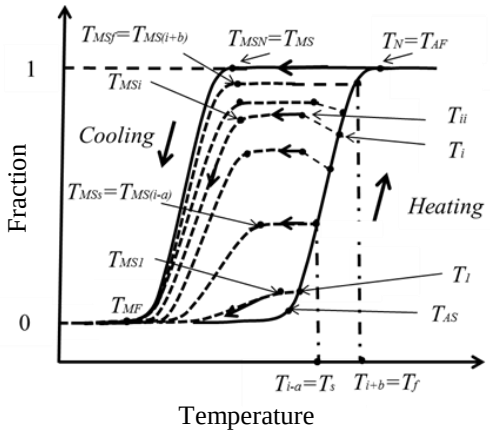

Figure. 2 Austenite fraction-temperature hysteresis

where ε_{ah} and ε_{ac} are the amount of austenite fractions during the heating and cooling processes; T_{MS} and T_{MF} are the initial and final temperatures of the martensite; T_{AS} and T_{AF} are the initial and final temperatures of the austenite, respectively.

As mentioned above, the Liang and Rogers model only represents the major hysteresis loop of the phase transformations without considering the martensite starting temperature of minor loops. A typical austenite fraction-temperature hysteresis schematic is shown in Fig. 2. The solid line represents the major hysteresis loop and the dashed lines are for minor hysteresis loops.

If $T_i \le T_{AS}$, then $\varepsilon_{ahi}(T)$=0, and therefore, only the case of $T_i > T_{AS}$ is considered. For a hysteresis loop, the austenite fraction ε_{ahi} during the heating process is expressed by

$$\varepsilon_{ahi}(T) = \begin{cases} 1 & T \ge T_i > T_{AF} \\ 0.5\left[1 - \cos \pi \left(\frac{T - T_{AS}}{T_{AF} - T_{AS}}\right)\right] & T_{AS} \le T < T_i \le T_{AF} \\ 0 & T \le T_i < T_{AS} \end{cases} \quad (4)$$

where $i = 1,2,3,\cdots,N$; T_i is the maximum temperature during the heating process of a hysteresis loop.

When $T_s < T_i < T_f$, then the austenite fraction increases, is maintained unchanged, and then decreases during the cooling process; the equation of the increase and maintaining stages ε_{acii} is expressed by

$$\varepsilon_{acii}(T) = \begin{cases} \varepsilon_{ahi}(T_i) + z_i(T) & T_{ii} < T < T_i \quad ,increasing \\ \varepsilon_{ahi}(T_i) + z_i(T_{MSi}) & T_{MSi} \le T \le T_{ii} \quad ,maintaining \end{cases} \quad (5)$$

where T_{ii} is the starting temperature of the maintaining stage; T_{MSi} is the martensite starting temperature of a minor hysteresis loop; $z_i(T)$, the function for the cooling process in the minor hysteresis loop, is expressed by

$$z_i(T) = \begin{cases} \frac{j_i(T_i - T)}{T_i - T_{ii}} & T_{ii} < T < T_i \\ z_i(T_{MSi}) = j_i & T_{MSi} \le T \le T_{ii} \end{cases} \quad (6)$$

where j_i is the constant for a minor hysteresis loop.

The martensite starting temperature T_{MSi}, which must be determined to model minor hysteresis loop, is expressed by

$$T_{MSi} = NT_{MSi}(T_{MS(i+b)} - T_{MS(i-a)}) + T_{MS(i-a)}$$

$$\text{and } T_{MS(i-a)} \le T_i \le T_{MS(i+b)} \quad (7)$$

where the normalized resistance NT_{MSi} is expressed by

$$NT_{MSi} = m_5 NT_i^5 + m_4 NT_i^4 + m_3 NT_i^3 + m_2 NT_i^2 + m_1 NT_i^1 + m_0 \quad (8)$$

where m_5 , m_4 , m_3 , m_2 , m_1 and m_0 are the parameters obtained by Matlab; the normalized resistance NT_i can be expressed by

$$NT_i = \frac{T_i - T_s}{T_f - T_s}, \ T_s \le T_i \le T_f \quad (9)$$

When $T_i \le T_s$ or $T_f \le T_i$, then $z_i(T) = 0$ and the martensite starting temperature T_{MSi} can be expressed by

$$T_{MSi} = q\ \varepsilon_{ahi}(T_i) + e \quad (10)$$

where q and e are the constants.

During the cooling process, the austenite fraction for a loop can be expressed by

$$\varepsilon_{aci}(T) = \begin{cases} \varepsilon_{acii}(T) & T_i \ge T > T_{MSi} \\ 0.5\left[1 - \cos\pi\left(\frac{T - T_{MF}}{T_{MSi} - T_{MF}}\right)\right]\varepsilon_{acii}(T_{MSi}) & T_{MF} \le T \le T_{MSi} \\ 0 & T < T_{MF} \end{cases} \quad (11)$$

C. *Mechanical model*

With the equations for the austenite fraction, the output displacement of the mechanical model D is expressed by

$$D = \begin{cases} g\ \varepsilon_{ahi} & heating \\ g\ \varepsilon_{aci} & cooling \end{cases} \quad (12)$$

where g is a constant.

III. Experimental setup and parameter identification

A. *Experimental setup*

An experimental setup of the proposed SMA actuator was made, and as shown in Fig. 3(a), the fixed end of the wire at the joint is connected to a load cell and the other end is attached to a bias spring. When the SMA wire is heated to the austenite length and the electric current is discontinued, the bias spring pulls the SMA wire back to the martensite length. A reflection sheet is connected to the spring for the displacement measurements. As the SMA wire shrinks and extends, the reflection sheet moves forward and backward. Fig. 3(b) is a photo of the experimental setup in Fig. 3(a); the displacement and force are obtained by a KEYENCE LC-2000 laser displacement meter and a TEDEA-HUNTLEIGH load cell, respectively. Details of the parameters in experiment are listed in Table 1.

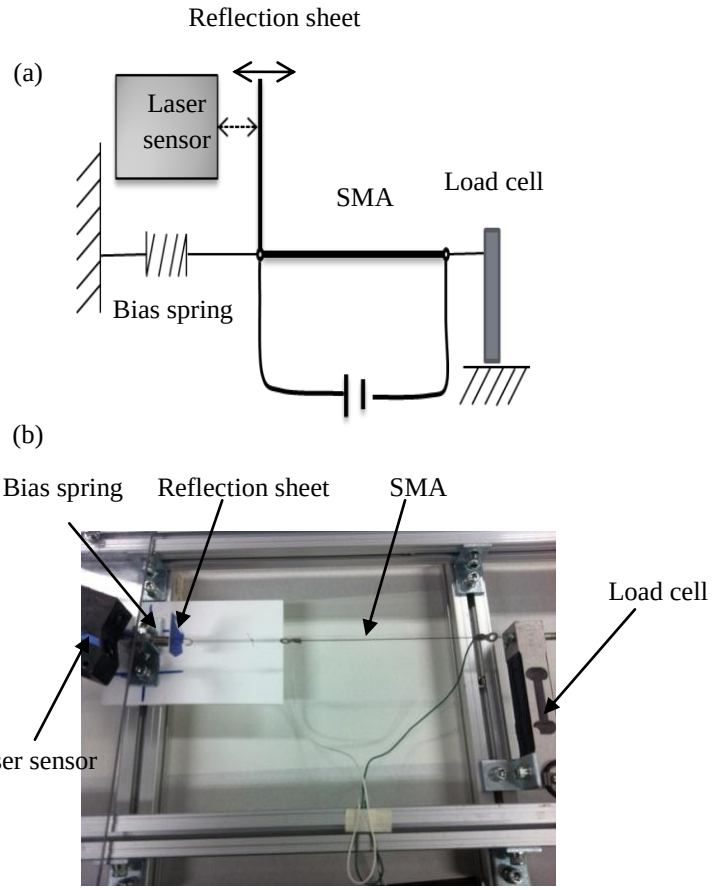

Figure. 3 (a) Schematic outline of the experimental setup
(b) Photo of the experimental setup

TABLE I. PARAMETERS OF THE EXPERIMENTS

Ambient temperature	22℃	SMA diameter	0.5 mm
MOSFET	K2232	SMA length	140 mm
Power supply	5 V	Spring stiffness	653.3 N/m
Microcontroller	Arduino	Pretension force	2.75 N

B. *Parameter identification*

To accurately identify the parameters of the modified Liang and Rogers model, the input voltage applied to the SMA actuator in the training process is a slow decaying ramp signal, making it possible to allow the temperature to stabilize. As shown in Fig. 4, the slopes of the decay reversal curves are set to $\pm 5.88\times10^{-3}$ in the training process of the modified Liang and Rogers model. Fig. 5 shows the results of simulations of the austenite fraction versus temperature, including the major and minor hysteresis loops for the SMA actuator. The six modified Liang and Rogers model parameters, identified by Matlab, are listed in Table 3. Based on the (7-10), the martensite starting temperature of minor loops T_{MSi} can be predicted. T_1 , T_2 , T_3 , T_4 , and T_5 are selected to identify the parameters in (7) , while T_1, T_5, and T_6 are for the parameters in (10). With the relationship between the austenite fraction and output displacement in (12), as shown in Fig. 6, the output with the modified Liang and Rogers model in the time domain is plotted together with the experimental data (colors other than red), including the major loop plotted in a red solid line and the minor loops plotted in red dashed lines. This figure clearly shows that the modified Liang and Rogers model can effectively characterize the hysteresis behavior of the SMA actuator.

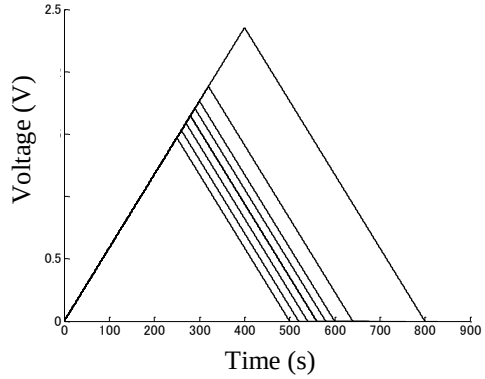

Figure. 4 Schematic of the input voltage

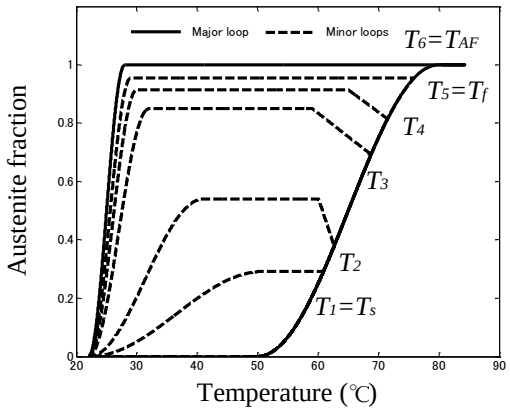

Figure. 5 Simulated values of the austenite fraction

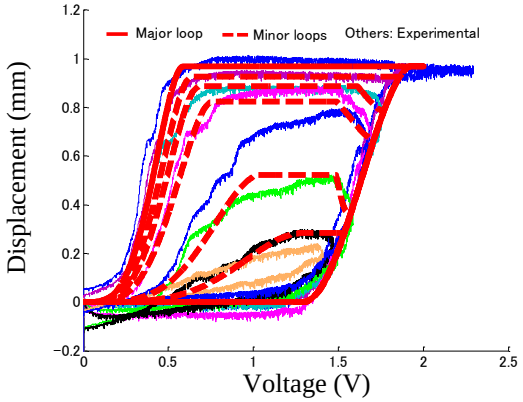

Figure. 6 Plot with experimental and simulated data versus temperature

TABLE II. PARAMETERS USED IN THE SIMULATION AND POSITION CONTROL

Parameter	Value	Parameter	Value
ρ	6500 kg m^3	R	1 Ω
h	165W/m^2℃	c	836.8 J/kg℃
m_5	2.2385	m_4	0
m_3	-8.6475	m_2	10.2425
m_1	-4.8334	m_0	1.0000
q	-32.6936	e	60.4657
T_{AS}	50.2℃	T_{AF}	80.1℃
T_{MS}	28℃	T_{MF}	22℃
T_{MSf}	28.9℃	T_{MSs}	51.1℃
j_f	0	j_s	0
ε_{ahf}	0.96	ε_{ahs}	0.29
T_f	75.9℃	T_s	60.8℃
T_{MS2}	40.8℃	T_{MS3}	32.1℃
j_2	0.16	j_3	0.19
ε_{ah2}	0.38	ε_{ah3}	0.66
T_2	63.1℃	T_3	68.5℃
T_{22}	61.2℃	T_{33}	59.1℃
T_{MS4}	30.1℃	T_4	71.5℃
j_4	0.1	T_{44}	65.2℃
ε_{ah4}	0.82	g	0.958

IV. Modified Liang and Rogers inverse model

To completely compensate the hysteresis effect of an SMA system, it is important to develop the exact inverse of the hysteresis model. Generally, as suggested in Fig. 7, for the

hysteresis model H and inverse model H^{-1}, the following equation can be developed if the inverse model exists [7].

$$y = H(v) = H(H^{-1}(u)) = u \tag{13}$$

here y is the output displacement of modified Liang and Roger model; v is the output voltage of the modified Liang and Roger inverse model which is used as the feedforward in the proposed control system; u is the input displacement.

A. *Inverse mechanical model*

The equations of the modified Liang and Rogers inverse model are briefly introduced to be applied as feedforward compensators to reduce the hysteresis effect of the SMA actuator. The inverse mechanical model which is derived from the mechanical model is expressed by

$$\varepsilon_{ahi/aci} = \frac{D}{g}, \quad \frac{dD}{dt} > 0 / \frac{dD}{dt} < 0 \tag{14}$$

where D is the input displacement; ε_{ahi} and ε_{aci} are the austenite fraction during the heating and cooling processes.

B. *Inverse phase transformation model*

Basic equations of output temperature for the inverse phase transformation model which are derived from the phase transformation model mentioned above are expressed by

$$T_{ahi} = \begin{cases} T_{AF} & \varepsilon_{ahi} > 1 \\ T_{As} + \frac{1}{\pi}(T_{AF} - T_{AS}) \arccos(1 - 2\varepsilon_{ahi}) & 0 \le \varepsilon_{ahi} \le 1 \\ T_{AS} & \varepsilon_{ahi} < 0 \end{cases} \tag{15}$$

$$T_{aci} = \begin{cases} T_{MSi} & \varepsilon_{aci} > \varepsilon_{acii} \\ T_{MF} + \frac{1}{\pi}[T_{MSi} - T_{MF}] \arccos(1 - \frac{2\varepsilon_{aci}}{\varepsilon_{acii}}) & 0 \le \varepsilon_{aci} \le \varepsilon_{acii} \\ T_{MF} & \varepsilon_{aci} < 0 \end{cases} \tag{16}$$

where T_{ahi} and T_{aci} are the output temperature of heating and cooling processes.

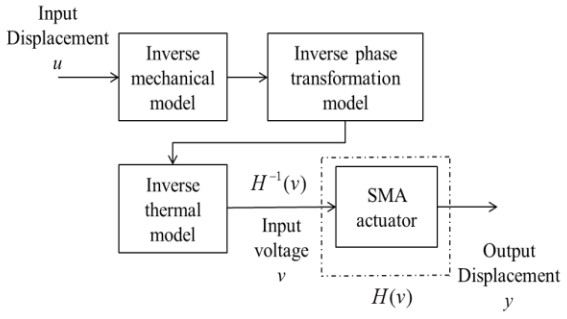

Figure. 7 Block diagram for the compensation based on the inverse model

C. *Inverse thermal model*

For a spring-biased SMA wire, the relationship between the input temperature T and the output voltage V of the inverse thermal model which is derived from the thermal model mentioned above is given by

$$V = \sqrt{R[\rho c \frac{\pi d_0^2 L_0}{4} \cdot \frac{dT}{dt} + \pi d_0 L_0 h(T - T_{amb})]} \tag{17}$$

To accurately control the position of the SMA actuator using the proposed control system, (7) and (10) are used to determine the martensite starting temperature T_{MSi}, which is used in (17) to calculate the input voltage of the major and minor hysteresis loops during the cooling process.

v. Control system based on the modified Liang and Rogers inverse model

As also mentioned above, much research has focused on control of the position of SMA actuators, including compensation for the hysteresis behavior using the hysteresis inverse model. Near the phase transformation region, the output displacement is sensitive to small changes in the applied voltage, and the proposed control system consists of both a closed-loop PID controller and an inverse compensator, to increase the accuracy of the tracking as well as to eliminate steady state errors in the position control of SMA actuator. As shown in Fig. 8, the block diagram of the proposed control system shows that the input displacement is used as the input of the modified Liang and Rogers inverse model. The output V_1 of the inverse model is the major portion of the input voltage to the SMA actuator. The total voltage applied to the SMA actuator is expressed by

$$V = V_1 + V_2, \quad 0 \le V \le 2V \tag{18}$$

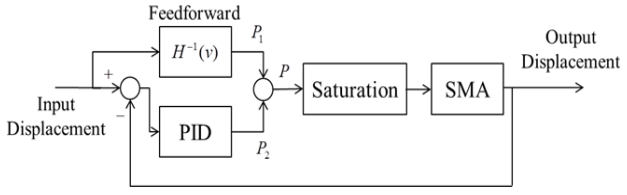

Figure. 8 Block diagram of the proposed control system based on the inverse model

VI. Experimental results

To show the effectiveness of the modified Liang and Rogers inverse model used in the proposed control system for the hysteresis compensation, two control cases are considered, a feedforward hysteresis compensation incorporated in a closed-loop PID controller and a traditional PID controller without feedforward hysteresis compensation. Two sets of input signals are selected and the results of each test are presented later in this section. Fig. 9 shows the results with the proposed controller and traditional PID controller using a multi-step as reference input. The figure clearly shows that the proposed method leads to less overshoot and more accurate tracking results than with the case where only the PID controller is used though both the systems in the test eliminate the steady state error. As shown in Fig. 10, it is observed that the error in the proposed method is smaller than with the traditional PID controller during both the heating and cooling processes. Fig. 11 shows the applied voltages of both control systems. In this figure, the range of variation in the voltage for the proposed controller is smaller than that of the traditional controller, which leads to reduce the tracking errors and achieves more accurate tracking results.

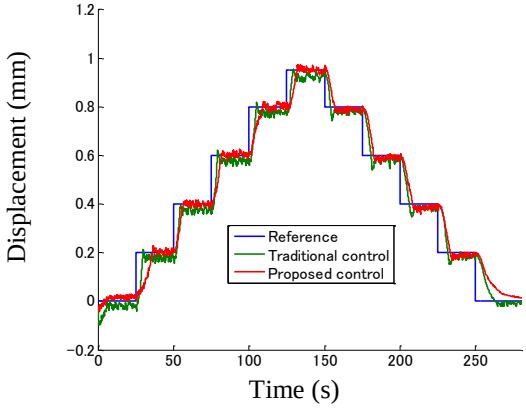

Figure. 9 Experimental results for test 1

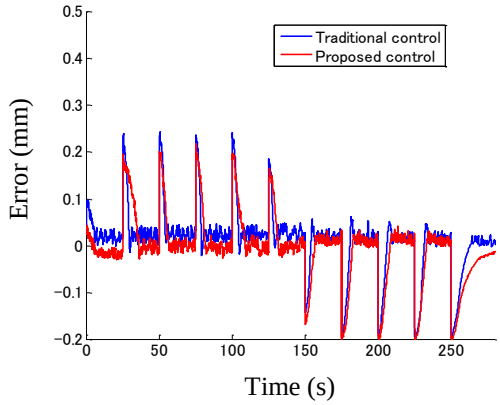

Figure. 10 Tracking errors for test 1

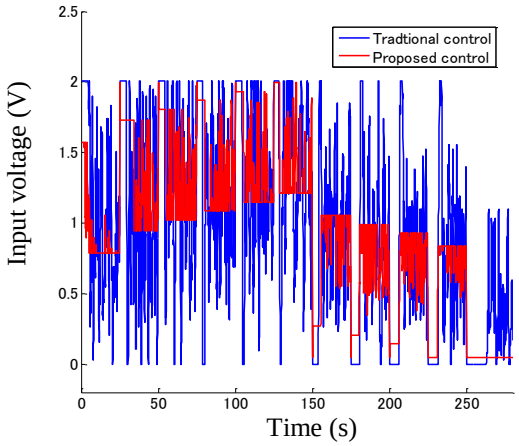

Figure. 11 Input voltage VS time plot for test 1

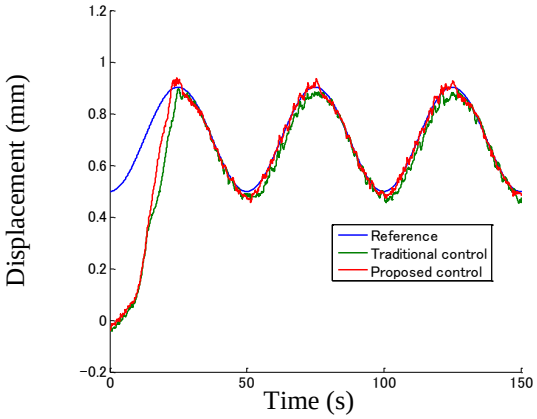

Figure. 12 Experimental results for test 2

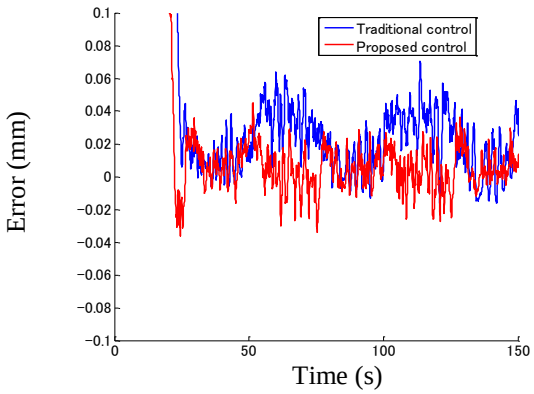

Figure. 13 Tracking errors for test 2

In the second experiment, a sinusoidal trajectory with fixed amplitude is used as the reference input signal to test the effectiveness of the proposed control system. As shown in Fig. 12, the experimental results of the proposed control system including the modified Liang and Rogers inverse model plus the PID controller result in better tracking accuracy than the conventional PID controller. This will be clearer when the

values of the position errors are depicted over time as in Fig. 13. During the cooling processes, from 75s to 100 s, and from 125 s to 150 s, the error of the proposed controller is smaller than the conventional controller; during the heating processes, from 50 s to 75s, and from 100 s to 125 s, the maximum absolute error of the proposed control system and the conventional controller are 0.070 mm and 0.034 mm, respectively. It means that the proposed controller improves the position error more than 50% (51.4%).

VII. Conclusions

In this paper, a newly developed control method based on the modified Liang and Rogers inverse model is proposed to reduce the hysteresis effect in the position control of an SMA actuator and the experimental results with the proposed control system behavior better than with only the traditional PID controller.

Based on the Liang and Rogers model, the modified Liang and Rogers model considering both major and minor hysteresis loops is developed and the model parameters are adjusted by an experimental identification procedure. The model developed here can predict the martensite starting temperature of minor hysteresis loops, successfully.

To obtain precise control and also to eliminate steady state errors, the modified Liang and Rogers inverse model, used as a feedforward compensator and incorporated with a PID controller, is applied to control the position of the SMA actuator. The experimental results of the multi-step reference show that using the proposed control system results in less overshoot and undershoot than with the traditional PID controller. The proposed control system also achieves a better tracking trajectory than the traditional controller when the reference input is a sinusoidal wave.

References

[1] M. Hashimoto, M. Takeda, H. Sagawa, I. Chiba, and K. Sat, "Shape memory alloy and robotic actuators, " J. Robot. Syst., vol. 2, pp. 3-25, 1985.

[2] KY. Tu, TT. Lee, CH. Wang, and CA. Chang, "Design of a fuzzy walking pattern (FWP) for a shape memory alloy (SMA) biped robot, " Robotica, vol. 17, pp. 373 -382, 1999.

[3] V. Michaud, "Can shape memory alloy composites be smart? , " Script. Mater, vol. 50, pp. 249-253, 2004.

[4] G. Gilardi, V. Bundhoo, E. Haslam, and EJ. Park, "A shape memory alloy based tendon-driven actuation system for biomimetic artificial fingers, Part II: Modeling and control, " Robotica, vol. 28, pp. 675‑687, 2010.

[5] V. Bundhoo, E. Haslam, B. Birch, and EJ. Park, "A shape memory alloy based tendon-driven actuation system for biomimetic artificial fingers, Part I: Design and evaluation, " Robotica, vol. 27, pp. 131‑146, 2009.

[6] JL. Pons, R. Ceres, and F. Pfeiffer, "Multifingered dexterous robotic hand design and control: a review, " Robotica, vol. 17, pp. 661‑674, 1999.

[7] S. Hassan, and R.Z. Mohammad, "Position control of shape memory alloy actuator based on the generalized Prandtl‑Ishlinskii inverse model. Mechatronics 2012;22(7):945‑57.

[8] C. Liang, and A. Rogers, "One-dimensional thermomechanical constitutive relations for shape memory materials, " Journal of Intelligent Material Systems and Structures, vol. 1, pp. 207-234, 1990.

About Author (s):

Junfeng Li is currently working toward the Ph.D in faculty of engineering, Hokkaido University, Sapporo, Japan. His research interests include control smart actuators and Robotics.

Hiroyuki, Harada received the B.S, M.S and Ph.D. degree from Hokkaido University, Sapporo, Japan. He is currently an associate professor of faculty of engineering. His research interests include control smart actuators, precision engineering, and Robotics.